Proceedings of the 7th International Symposium on Cavitation
CAV2009 - Paper No. 97
August 17-22, 2009, Ann Arbor, Michigan, USA

A BOUNDARY ELEMENT METHOD FOR THE STRONGLY NONLINEAR ANALYSIS OF SURFACE-PIERCING HYDROFOILS

Vimal Vinayan*
Ocean Engineering Group
Department of Civil, Arch. and Env. Engineering
University of Texas at Austin
Austin,Texas 78712
Email: vvinayan@mail.utexas.edu

Spyros A. Kinnas
Ocean Engineering Group
Department of Civil, Arch. and Env. Engineering
University of Texas at Austin
Austin,Texas 78712
Email: kinnas@mail.utexas.edu

ABSTRACT

A two-dimensional BEM scheme is presented for the numerical modeling of the ventilated flow past a surface-piercing hydrofoil. Fully nonlinear boundary conditions are applied on the free-surface which allows for the accurate modeling of the jets generated on the wetted boundaries as a result of the passage of the hydrofoil through the air-water interface or the free-surface. The scheme is validated through a comparison with self-similar solutions in the case of non-ventilating symmetric water-entry and with experiments in the case of ventilating entry. In addition, a multi-phase RANS model (FLUENT based) is used to gauge the effects of viscosity and the formation of spray. Results are presented for the fully wetted and ventilating cases with and without the effects of gravity, simulating the effect of a change in the Froude number. Results are also presented for the case of a hydrofoil in rotational motion, simulating the ventilation characteristics at the radial section of a typical surface-piercing propeller. The fully nonlinear scheme presented here is a step towards assessing the errors associated with some of the linear free-surface assumptions made in a 3D BEM tool (PROPCAV) for the performance prediction of surface-piercing propellers.

INTRODUCTION

Surface-piercing propellers (hereafter referred to as SP propellers) and waterjets are the two commonly used systems of propulsion for high-speed crafts (vessels that operate routinely at speeds in excess of 30 knots [1], [2]). Cavitation and its detrimental effects of loss of thrust, noise, vibration and erosion present a formidable barrier that precludes the use of subcavitating or supercavitating propeller based systems. Even though it is difficult to draw a clear demarcation between the two modes of propulsion in terms of feasibility, current trends indicate the prevalence of SP propellers for high-speed crafts with displacements below 50 t while waterjets are used for crafts with higher displacements [3].

The elements of the surface-piercing propulsion system are arranged in such a manner that when the vessel is underway, only a part of the propeller is submerged during a cycle of revolution (the actual level of submergence depends on the trim of the vessel and other factors). SP propellers are also referred to as partially-submerged propellers because of this feature. Some of the advantages offered by such an arrangement, which in turn translate to better propulsive efficiency and extended range of operation are : (i) there is a considerable reduction in the appendage drag due to the absence of submerged components like shafts, struts, etc. (ii) a reduction in the detrimental effects of cavitation as it is replaced by natural ventilation, and (iii) the absence of diameter limitations imposed by draft and hull clearance requirements. In spite of being an efficient system of propulsion, the design of partially submerged propellers has often been performed on a trial-and-error basis with full-scale propellers or based on experimental results from model tests [4]. Both these methods have their disadvantages - (i) design based on full-scale propellers do not provide information about the dynamic blade loads nor the average propeller forces [4], (ii) model test based designs are prohibitively expensive to carry out and are prone to scale effects [5, 6], and are also influenced by the test techniques [7, 8].

The widespread use of SP propellers underscores the importance of developing reliable numerical tools for predicting their performance. The numerical modeling of the real flow associated with a SP propeller is too difficult a task to undertake. Young & Kinnas (2003) [9, 10] note the difficulties - (i) insufficient understanding of the physical phenomena involved at the entry and exit phases of the blade passage through the air-water interface, (ii) insuffi-

*Address all correspondence to this author.

cient understanding of the dynamic loads associated with the propeller piercing the water surface at high speeds, (*iii*) the modeling of long ventilated cavities that extend into the wake of the propeller, which also get interrupted by the free-surface, (*iv*) the modeling of jets formed along the pressure side and the associated increase in the free-surface elevation at the instance of blade entry and exit, (*v*) the effect of blade vibrations due to cyclic loading (in water) and unloading (in air) of the propeller. With the above-mentioned issues, the numerical modeling of SP propellers can only be realized through a series of simplifying assumptions.

Young & Kinnas (2003) [10] developed a numerical method to predict the performance of SP propellers that also included the nonlinear analysis of unsteady sheet cavitation/ventilation with the propeller subject to a time-dependent inflow. The method was developed over an existing robust numerical tool PROPCAV (PROPeller CAVitation, [11]) so named for its ability to solve the 3-D unsteady flow around cavitating propellers. PROPCAV is based on a low-order (piecewise constant dipole and source distribution) potential boundary element method (BEM) and the method of Young & Kinnas (2003) [10] allowed it to determine the shape of the ventilated cavity surface created as a result of the passage of the blades of a SP propeller from air to water. A detailed review of the lifting line and lifting surface based numerical methods developed prior to the PROPCAV model is given in Young (2002) [9]. The simplifying assumptions made in the 3-D hydrodynamic model are as follows: (*i*) the Froude number is assumed to be very large and thus the effects of gravity are neglected (*ii*) the free-surface jets formed as the blade enters and exits the free-surface are assumed to be negligible (i.e. the free-surface is treated as a flat surface and its effect is taken into account using the negative image method), (*iii*) the cavities are assumed to be fully ventilated, i.e. the pressure on the cavity is constant and equal to the atmospheric pressure. The ventilated cavity detachment locations are searched for on the suction (back) side of the blade, (*iv*) the wake is assumed to be a helical surface with constant pitch and radius,(*v*) the influence of the shed and trailing vorticity in the wake once the blade has left the free-surface is assumed to be negligible.

Young & Kinnas (2003) [10] applied the PROPCAV model to the `841-B` propeller tested by Olofsson (1996) [4]. In spite of the simplifying assumptions, the predicted ventilation patterns agreed well with the measured (experimental) results. Figure 1 (from [9]), shows a representative comparison of the predicted and measured blade forces for an advance ratio (J_A) of 0.8. In comparison to the experimental results, PROPCAV predicts the mean forces with reasonable accuracy. However, the following discrepancies can be observed:

(1) A significant difference exists between the predicted and measured forces during the entry phase. With reference to Figure 1, the entry phase approximately corresponds to the blade angle range of 75° to 120°. This difference, but of lesser magnitude, exists even in the case of higher advance ratios.

(2) The experimental results show "humps" in the blade forces. Olofsson (1996) [4] attributes this to blade resonance effects as a result of the cyclic loading and unloading of the propeller. This behaviour is not captured by the PROPCAV model as it assumes the propeller to be rigid.

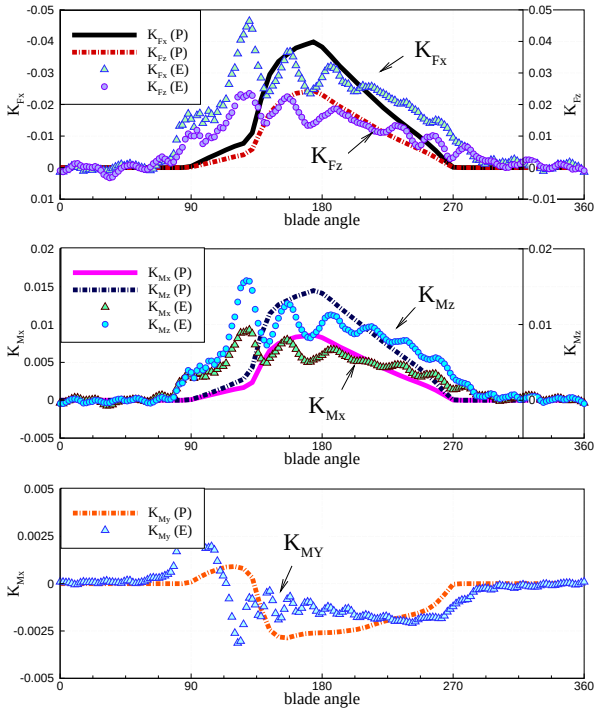

Figure 1: Comparison of predicted (P) and measured (E) blade forces for $J_A = 0.8$.

The authors are of the opinion that the difference in forces at the entry-phase is primarily due to the inability of the 3-D model to capture the nonlinear effects of the free-surface. Vibration of the blade, the other cause of the difference in forces, tends to become important only after the blade has fully submerged. The authors feel that prior to including any effects of blade-vibration, the free-surface model in PROPCAV should be improved.

It was mentioned earlier that including the whole gamut of nonlinear free-surface effects in the 3-D model would entail considerable effort. The authors feel that it is pru-

dent to focus first on a systematic study of a 2-D surface-piercing hydrofoil or more appropriately a blade element of a SP propeller with fully nonlinear free-surface conditions. This study is along the lines of the 2-D approach introduced by Yim (1974) [12] and later extended by Wang (1977,1979) [13, 14]. The insight gained through the 2-D study can be used as a basis for improving the 3-D model. The objectives of the 2-D study are :

(1) *Quantify the effects of the Froude number* : The Froude number, defined as $F_n = nD/\sqrt{gD}$ with D being the diameter of the propeller and n the rate of revolution, essentially measures the influence of gravity, g. The effect of gravity is negligible in the fully ventilated regime (at low advance ratios) when $F_n > 3$([4], [15]). However, in the partially ventilated regime (at high advance ratios), the Froude number can have an effect on the overall ventilation characteristics. Moreover, each section of the propeller operates at a different "local" Froude number. The 2-D model can be used to identify sections that could either partially or fully ventilate.
(2) *Quantify the added hydrodynamic forces* due to nonlinearity of the free-surface and the ventilated cavity surface.

2-D SURFACE-PIERCING HYDROFOILS

The problem of a 2-D surface piercing hydrofoil can be classified under the category of water entry of bodies and slamming. Water-entry has been studied extensively over the years following the seminal works of Von Karman (1929) [16] and Wagner (1932) [17]. A review of the subject can be found in [2] and [18]. Both analytical (self-similar solutions) and various numerical solutions have been developed over the years for both small and large deadrise angles. A critical difference between the study of slamming and the entry of surface-piercing hydrofoils is the possibility of ventilation, either partial or complete, at sufficiently large angles of attack. A key similarity is the generation of free-surface jets along the wetted part of the body. In the context of ventilating surface piercing hydrofoils, Yim (1974) [12] applied a linearized theory to study the water entry and exit of a thin foil, and a symmetric wedge with ventilation. Similar linearized theories were put forward by Cox (1971) [19], Terentev (1977) [20] and Wang (1977,1979) [13, 14]. Cox (1971) [19] also conducted a series of experiments on a surface piercing hydrofoil (wedge-shaped) at different angles of attacks and velocity of entry. Chekin (1989) [21] and more recently Faltinsen (2008) [22] put forward a nonlinear theory for the water-entry of a ventilating flat-plate. A recurring theme in the existing linear and nonlinear theories of ventilated entry is the *absence of gravity* (similarity solution) and application to relatively *simple geometries* (flat plates, circular arcs).

This section presents the potential Boundary Element Method (BEM) based scheme used to model the water entry of a surface-piercing hydrofoil. The BEM scheme used here was developed initially in the context of the roll-motion of FPSO hull-sections. Only a brief summary of the mathematical and numerical formulation is presented here and the complete details of the scheme can be found in Kinnas (2005) [23] and Vinayan (2007) [24]. In essence the problem is formulated as an initial boundary value problem (IBVP) for a velocity potential that satisfies the Laplace equation. The IBVP is solved by combining the mixed Eulerian-Lagrangian method of Longuet-Higgins & Cokelet (1976) [25], for tracking the free-surface, with the solution of a Boundary Integral Equation (BIE) at each time-step. The current numerical scheme offers the advantage that it can be applied to entry/exit of arbitrarily shaped SP propeller sections or hydrofoils with and without the effects of gravity.

Previous numerical work

Savineau & Kinnas (1995,1996) [26, 27] solved the flow field around a fully ventilated two-dimensional surface-piercing hydrofoil using a time-marching low-order boundary element method. The numerical tool, called SPPAN, solved for the shape of the ventilated cavity and the pressure on the surface of the hydrofoil in the entry-phase. The important characteristics of the method are (i) the flow is solved with respect to a coordinate system that moves along with the foil, (ii) the vertical velocity of entry is assumed to be sufficiently high for ventilation to start at the sharp leading edge of the foil and form a cavity along the suction side. (iii) an infinite Froude number is assumed and with this assumption, the free-surface boundary conditions are linearized and the effects of gravity neglected. (iv) the total potential, hence the velocity field, is decomposed into inflow and perturbation components. A boundary-value problem is solved to obtain the perturbation potential at each time-step of the time-marching scheme, (v) the linearized free-surface boundary conditions are enforced using a "*negative*" image method, and (vi) the ventilated cavity shape is found iteratively by aligning the panels with the flow and at convergence the cavity surface is tangent to the flow.

Current work - Mathematical Formulation

Consider a rigid, 2-D hydrofoil entering an initially calm domain with a constant velocity $\vec{V}$ and an angle of attack α, as shown in Figure 2. An ideal fluid is considered and the flow is assumed to be irrotational. A *fixed* (non-rotating) Cartesian coordinate system is chosen to represent the flow with its origin at the undisturbed water level. The flow is represented in terms of a harmonic function $\phi(\mathbf{x}, t)$ commonly referred to as the

velocity potential. Also, the local fluid velocity is given as $\vec{q}(\mathbf{x},t) = \nabla\phi = (\phi_x, \phi_y) = (u, v)$. Here, $\mathbf{x} = (x, y)$ represents the spatial location with respect to the fixed coordinate system, with x being the horizontal measure and y the vertical measure positive upward. The fluid domain and the corresponding boundary surfaces are shown in Figure 2. $S_{\mathbb{WB}}(t)$ represents the "*wetted*" part of the hydrofoil surface, $S_{\mathbb{F}}(t)$ is the free-surface that also includes a part of the ventilated surface on the suction side of the hydrofoil and S_∞ is the far-field boundary placed *far* enough to minimize interference.

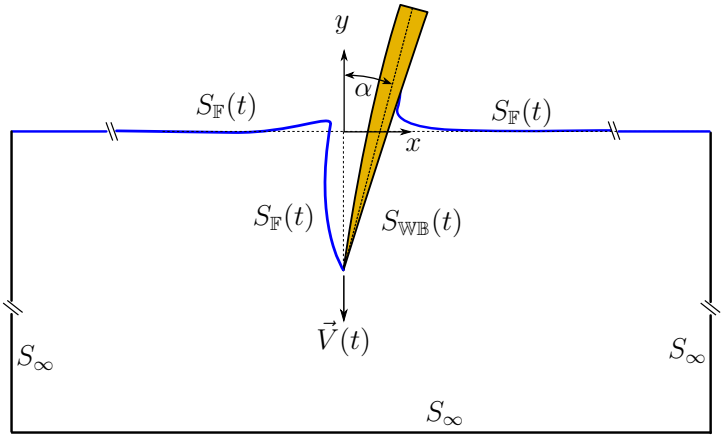

Figure 2: Entry of a surface-piercing wedge : Fluid domain and corresponding boundaries

• *Boundary Integral Equation*

A Boundary Integral Equation (BIE) is solved at each time-step of a higher-order time-stepping scheme in order to obtain the velocity potential. Once the solution is obtained for a particular time, the time-dependent boundary conditions are updated and the solution scheme progresses onto the next one.

The BVP for the velocity potential is converted into a BIE by introducing a two-dimensional Green's function $G(\mathbf{p},\mathbf{q}) = -\frac{1}{2\pi}\ln r_{\mathbf{pq}}$ (satisfies the Laplace equation), where $r_{\mathbf{pq}} = |\mathbf{p}-\mathbf{q}|$, $\mathbf{p} \equiv \mathbf{p}(\mathbf{x})$ is the field point and $\mathbf{q} \equiv \mathbf{q}(\mathbf{x})$ is the source point. The BIE obtained by applying Green's third identity to $\phi(\mathbf{x},t)$ and $G(\mathbf{p},\mathbf{q})$ is

$$\alpha(\mathbf{p})\phi(\mathbf{p}) + \int_\Gamma \phi(\mathbf{q}) G_n(\mathbf{p},\mathbf{q})\, d\Gamma_{\mathbf{q}} = \int_\Gamma G(\mathbf{p},\mathbf{q})\phi_n(\mathbf{q})\, d\Gamma_{\mathbf{q}} \qquad (1)$$

where $2\pi\alpha(\mathbf{p})$ is the internal angle formed at the boundaries. $G_n(\mathbf{p},\mathbf{q}) = \nabla G(\mathbf{p},\mathbf{q})\cdot\vec{n}_{\mathbf{q}}$ and $\phi_n(\mathbf{p},\mathbf{q}) = \nabla\phi(\mathbf{p},\mathbf{q})\cdot\vec{n}_{\mathbf{q}}$ and $\vec{n}_{\mathbf{q}}$ is the normal vector at $\mathbf{q}$, positive out of the fluid.

• *Kinematic Boundary Condition on $S_{\mathbb{F}}(t)$:*

The KBC is obtained by assuming $S_{\mathbb{F}}(t)$ to be a bounding surface, i.e., no material passes across the free-surface [28]. Based on the schematic shown in Figure 3, if we represent the free-surface as $F(\mathbf{x},t) = y - \eta(x,t) = 0$, the KBC on the free-surface is given as [28, 29]

$$\frac{D}{Dt}F(\mathbf{x},t) = 0 \qquad (2)$$

where $\frac{D}{Dt} = \frac{\partial}{\partial t} + \nabla\phi\cdot\nabla$ is the material derivative. $\vec{q} = \nabla\phi = (\phi_x, \phi_y)$ is the fluid velocity on the free-surface, and $y = \eta(x,t)$ is the free-surface elevation.

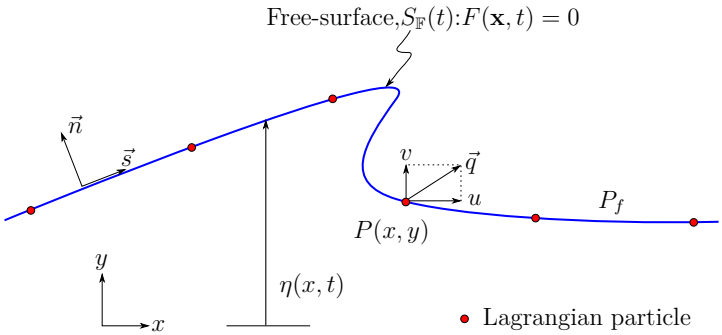

Figure 3: Free-surface schematic

From a Lagrangian particle representation of the free-surface, for a particle $P(x,y)$ on the free-surface, the KBC is given as [25, 28, 29]

$$\frac{D\mathbf{x}}{Dt} = \nabla\phi \quad \text{or} \quad \left\{\begin{array}{l} \frac{Dx}{Dt} = u = \phi_x \\ \frac{Dy}{Dt} = v = \phi_y \end{array}\right\} \quad \mathbf{x} \in S_{\mathbb{F}}(t) \qquad (3)$$

The dynamic boundary condition (DBC) is obtained from the Bernoulli's equation and assuming the pressure to be continuous across the free-surface. It is assumed that the wavelength of the free-surface elevation is long enough to neglect the effects of surface tension. Thus the pressure underneath the free-surface must equal the atmospheric pressure above giving the most general form of the free-surface DBC

$$\frac{\partial\phi}{\partial t} + \frac{1}{2}|\nabla\phi|^2 + g\eta + \frac{P_f}{\rho} = 0, \quad \mathbf{x} \in S_{\mathbb{F}}(t) \qquad (4)$$

where g is the acceleration due to gravity. The common form of the DBC is obtained by expressing the pressure as gage pressure, in which case the pressure on the free-surface, $P_f = P - P_{atm} = 0$. For a Lagrangian particle $P(x, y)$, the DBC can be rewritten as

$$\frac{D\phi}{Dt} = \frac{1}{2}|\nabla\phi|^2 - g\eta, \quad \mathbf{x} \in S_{\mathbb{F}}(t) \tag{5}$$

• *Boundary Condition on Hydrofoil* $S_{\mathbb{WB}}(t)$

On the "wetted" part of the hydrofoil surface $S_{\mathbb{WB}}(t)$,

$$\nabla\phi \cdot \vec{n} = \vec{V}(t) \cdot \vec{n}, \quad \mathbf{x} \in S_{\mathbb{WB}}(t) \tag{6}$$

where $\vec{V}(t)$ is the prescribed velocity of the hydrofoil.

• *Boundary Condition on Far Field Boundary* S_∞

The far-field boundary S_∞ is assumed to be a no-flux surface with

$$\nabla\phi \cdot \vec{n} = 0; \quad \mathbf{x} \in S_\infty \tag{7}$$

and special attention is paid to place the boundary far away from the body to avoid reflection of the waves generated its motion.

• *Initial Conditions*

The initial conditions for this problem depend on the angle of attack α and the existence of a ventilated cavity on the suction side of the hydrofoil.

(a) For a fully wetted flow, a tiny fraction of the wedge is assumed to be initially immersed. The solution is started impulsively and allowed to progress until the hydrofoil is completely immersed.

(b) The treatment of the fully ventilating case requires special attention. For a hydrofoil with a sharp leading edge, ventilation is triggered right at the leading edge. However, during the process of the development of the method it was found extremely difficult to numerically *trigger* ventilation at the leading edge. According to [13] the flow field surrounding a ventilating foil is identical to that of supercavitating flat plate (in an unbounded fluid domain) with zero cavitation number. This aspect of the flow forms the basis for getting the initial conditions for the ventilating flow. The proposed model consists of the following steps : (i) Assume an initial shape of the ventilated cavity - the initial shape is derived from the analytical expressions for the super-cavity produced by a flat plate in an infinite flow domain. These expressions are obtained from the free-streamline theory of [30]. The initial cavity length is assumed to be a fraction of the chord-length of the hydrofoil. (ii) Instead of being treated as a free-surface, the initial shape of the ventilated cavity is assumed to be rigid or wetted. With this assumption, the free-surface problem is solved as an asymmetric water entry. (iii) After the hydrofoil has traveled a certain extent, a part of the initial cavity assumed to be wetted is appended to the adjoining free-surface. (iv) The actual solution of the ventilating problem starts from this point onwards. The intersection of the initial ventilated cavity (modeled as wetted) and the free-surface is treated as a fixed separation point. The solution is allowed to progress with the free-surface on the suction side continuously detaching from the intersection point.

• *Treatment at a fixed separation point*

At the fixed separation point, the normal velocity of the free-surface is assumed to be the same as that of the hydrofoil. This assumption assures continuity of slope between the wetted body and the ventilated surface. This is consistent with the analytical solution for the local flow presented in [2] and [31]. The potential is inherently continuous by virtue of the use of linear isoparametric elements. The boundary integral equation is not solved at the separation point as both the primary variable (ϕ) and the secondary variable (ϕ_n) are known.

Current work - Numerical Formulation

A brief summary of the important numerical aspects of the scheme is presented here.

(a) A mixed Eulerian-Lagrangian (MEL) scheme of [25] is used to solve the initial boundary value problems presented in the previous chapter. The MEL scheme comprises primarily of two steps (1) solve a well-defined boundary value problem based on a given set of boundary conditions using the Boundary Element Method (BEM) and, (2) update the free-surface geometry and potential on the free-surface by time integration of the fully nonlinear kinematic and dynamic free-surface boundary conditions. These two steps are repeated at each time-step of a fourth-order Runge Kutta time marching scheme. The proper implementation and solution of the two MEL steps dominate the numerical implementation of the free-surface problem.

(b) Linear iso-parametric elements form the basis for the numerical solution of the boundary integral equation. A *double node* approach is used at the corners of the domain. However, the boundary integral equation is not solved at a *double node* if it happens to be a separation point.

(c) The treatment of the jet that forms along the wetted side of the hydrofoil is similar to that presented in [32] and [33]. The jet is allowed to grow until a threshold

angle is reached between the jet and the adjoining body surface. Once this limiting angle is reached a new panel is created at an angle larger than the threshold value. The intersection of the new panel with body surface becomes the new body- free-surface intersection point. The angle is continuously monitored during the solution and the *cut-off* process is implemented every time it is smaller than the threshold value. The value of the threshold angle is chosen to be $\frac{\pi}{15}$, a value chosen in par with the analytical solutions presented in [34].

(d) A re-paneling scheme is implemented to maintain sufficient and uniform resolution in the area of the jet. Even though linear elements are used to model the free-surface, re-paneling is performed using a cubic spline scheme with the arc-length of the surface as a parameter instead of the Euclidean distance. The arc-length is calculated by first fitting a cubic-spline with the node index as a parameter. With the cubic spline coefficients, the arc-length is calculated numerically using a twelve-point Gauss-Legendre quadrature. This approach was suggested in [25] to maintain the accuracy of the re-paneling scheme.

(e) A third-order five point least squares model is implemented to smooth instabilities that arise during the simulation. The smoothing scheme was found to be necessary to smooth out oscillations resulting from the impulsive start of the wetted problem. Since smoothing is an *artificial* process, it is used sparingly and applied only at an interval of 10 time-steps. Moreover, the smoothing process is applied only close to the intersection between the free-surface and the hydrofoil.

(f) The pressure on the body surface is obtained from the Bernoulli's equation

$$\frac{P}{\rho} = -\frac{\partial \phi}{\partial t} - \frac{1}{2}|\nabla \phi|^2 - gy \tag{8}$$

The critical part of this expression for the pressure is the evaluation of the time derivative $\frac{\partial \phi}{\partial t}$. In particular it is important to note that the body surface changes with time and also due to re-gridding. Taking these factors into consideration, we have

$$\frac{\delta \phi}{\delta t} = \frac{\partial \phi}{\partial t} + \vec{V_g} \cdot \nabla \phi \tag{9}$$

$\vec{V_g}$ is the local grid velocity of the body surface and represented as

$$\vec{V_g} = \left(\frac{\delta x_g}{\delta t}, \frac{\delta y_g}{\delta t} \right) \tag{10}$$

From (8) and (9), we have

$$\frac{P}{\rho} = -\frac{\delta \phi}{\delta t} + \vec{V_g} \cdot \nabla \phi - \frac{1}{2}|\nabla \phi|^2 - gy \tag{11}$$

The derivatives $\frac{\delta \phi}{\delta t}$, $\frac{\delta x_g}{\delta t}$ and $\frac{\delta y_g}{\delta t}$ are calculated as a part of the fourth-order Runge Kutta scheme based on the scheme of [35]

RESULTS

The subsequent sections present the results for the fully-wetted (non-ventilating) entry, ventilating hydrofoil (vertical entry) and ventilating hydrofoil in rotational motion.

Fully wetted entry

Similarity solutions ([36], [37]) exist in the case of water-entry of symmetric wedges and provide a valuable set of results for validating the current numerical algorithm. The BEM method is used to simulate the water entry of a symmetric wedge, in the absence of gravity, for different deadrise angles (also expressed in terms of the included wedge angle α_w). The scheme is allowed to progress until a state of self-similarity is reached and the results are compared with the corresponding analytical solutions of [36]. Figures 4,6 and 8 show the free-surface elevation in terms of the similarity variables for the deadrise angles of 81°, 60° and 45° respectively. Figures 5,7 and 9 show the comparison between the predicted pressure coefficients and that obtained from the similarity solution of [36]. The pressure coefficient is defined as $C_p = (P - P_{atm})/(0.5\rho V_w^2)$ where V_w is the entry velocity of the wedge. In all the cases, the correlation between the numerical and analytical pressures is excellent.

Apart from validating the numerical algorithm, the fully wetted scheme serves the following purposes:

(i) Simulate the entry of surface-piercing hydrofoil at small angles of attack when ventilation is not expected.

(ii) Provide an initial solution for the ventilating case.

Ventilating Hydrofoil - Vertical Entry

Cox (1971) [19] conducted a series of experiments with a symmetric wedge of dimensions 0.5" (12.7 mm) by 6" (152.4 mm) with a chord length of 6". In the experiments, the wedge was dropped from different heights (equivalent to changing the velocity of entry V_w) and at different angles of attack, α. For each instance, the ventilated cavity shape was photographed after the wedge had approximately traveled its length through the water surface. These photographs provide an excellent source of validation for the BEM model. As a representative case, a velocity of entry of 2.45 m/s

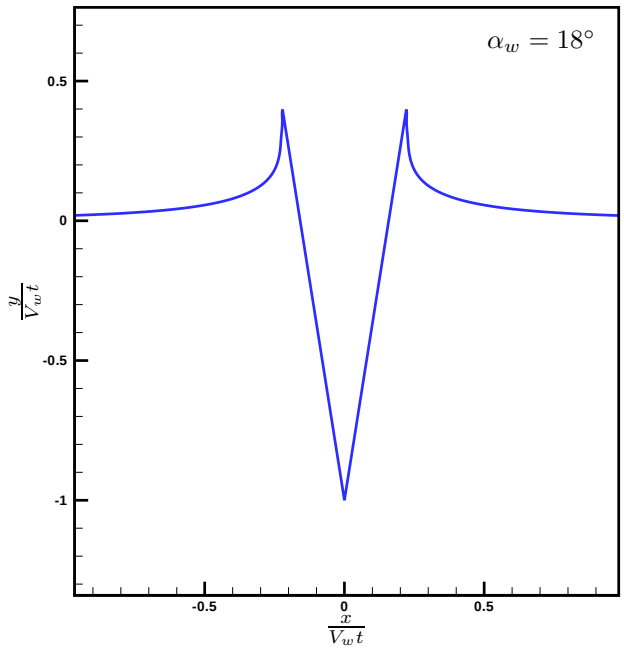

Figure 4: Free-surface elevation expressed in terms of similarity variables, included wedge angle $\alpha_w = 18°$ (deadrise angle = 81°)

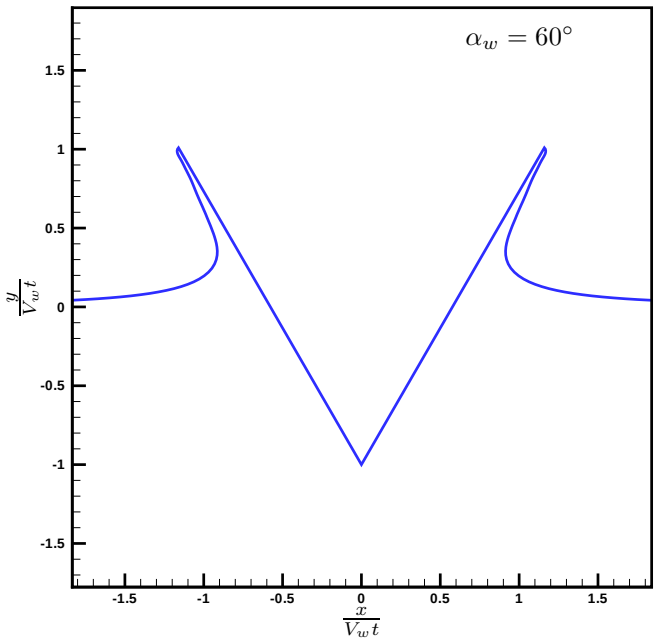

Figure 6: Free-surface elevation expressed in terms of similarity variables, included wedge angle $\alpha_w = 60°$ (deadrise angle = 60°)

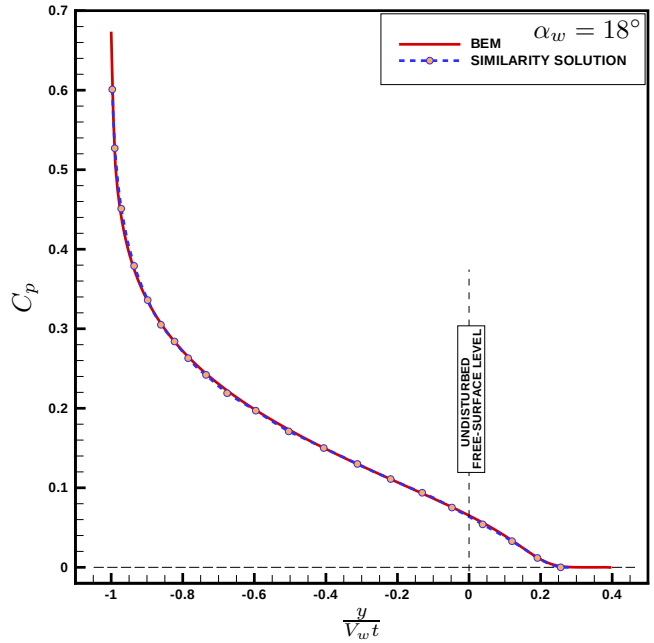

Figure 5: Comparison of predicted pressure with similarity solution, included wedge angle $\alpha_w = 18°$ (deadrise angle = 81°)

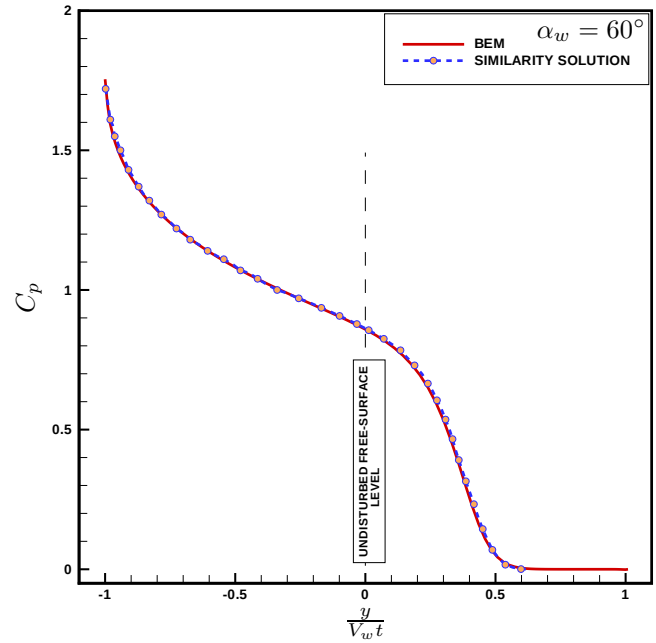

Figure 7: Comparison of predicted pressure with similarity solution, included wedge angle $\alpha_w = 60°$ (deadrise angle = 60°)

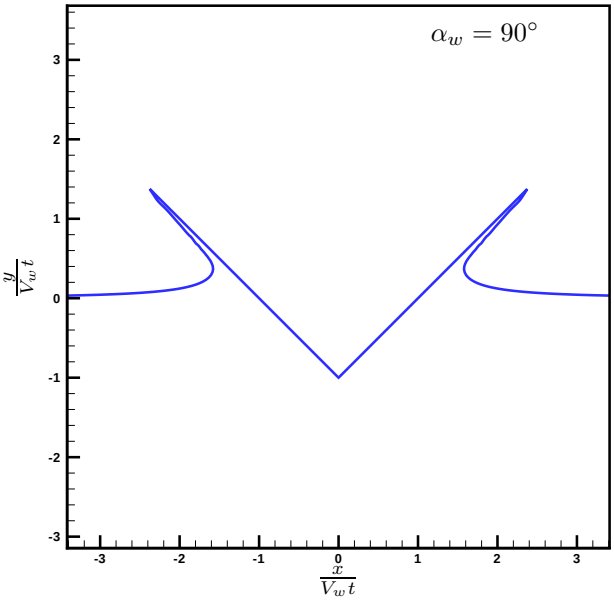

Figure 8: Free-surface elevation expressed in terms of similarity variables, included wedge angle $\alpha_w = 90°$ (deadrise angle = 45°)

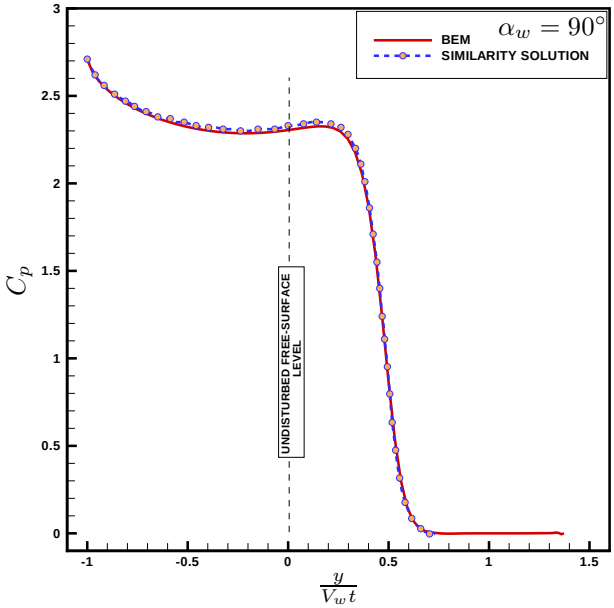

Figure 9: Comparison of predicted pressure with similarity solution, included wedge angle $\alpha_w = 90°$ (deadrise angle = 45°)

(corresponding to a drop of 12") is chosen for validation. All the subsequent BEM results correspond to this geometry and velocity.

It was mentioned in the numerical formulation that an initial guess for the ventilated cavity shape is obtained from corresponding solution of a supercavitating flat plate. The length of the initial guess is expressed as a percentage of the total chord (c) of the hydrofoil and is represented by the parameter δ_{iv}. Figure 10 shows the effect of the parameter δ_{iv} on the final ventilated cavity shape (the simulation is stopped once the free-surface on the wetted side reaches the base of the hydrofoil). In terms of a chord length c = 152.4 mm, the minimum δ_{iv} of 2% would be about 3mm, while the maximum would be about 7mm. On the whole, the parameter δ_{iv} does not effect the final shape of the ventilated cavity and the free-surface elevation on the wetted-side. Differences are observed in the region where the ventilated cavity meets the initially undisturbed free-surface. The similarity solution of [21] and [22] predict a cusp at the point where the two convex free-surfaces meet. This aspect of the flow is not considered in the numerical scheme and leads to the observed differences. Figure 11 shows the effect of δ_{iv} on the wetted-side pressure and no discernible differences are observed. (All the subsequent calculations are with $\delta_{iv} = 2\%c$.)

Figures 12 and 14 respectively show the ventilated cavity surfaces, shown for different levels of submergence, without ($g = 0$) and with ($g \neq 0$) the effects of gravity. Defining a Froude number in terms of the chord length c as $Fn_c = V_w/\sqrt{gc}$, $g = 0$ would correspond to $Fn_c = \infty$ and $g \neq 0$ to Fn_c=2. (Note that in the figures, only the wetted boundary of the hydrofoil is shown. Although the thickness form is not shown, the ventilated cavity does not intersect the suction side of the hydrofoil). The effect of gravity becomes apparent when the free-surface elevations are expressed in terms of the similarity variables as shown in Figures 13 and 15. In the absence of gravity (Figure 13) all the free-surface profiles, starting with the first instance when similarity is observed to the end of the simulation, are seen to overlap. The scheme is able to preserve the self-similarity of the flow. The lack of self-similarity, as expected, can be observed in Fig. 15 when the effect of gravity is included.

Figure 16 shows a comparison between the predicted cavity surface and that observed from the experiments of Cox (1971) [19] for an angle of attack of 10°. The free-surface elevations and the ventilated surfaces are compared at the same level of submergence. The overall agreement between the experiment and the numerical results is good.

Olofsson (1996) [4] mentions that in the fully ventilated regime, the effect of the Froude number is negligible when $Fn > 3$. This is because the ventilated cavities have asymptotically attained their final shapes and a subsequent increase in the Froude number makes no difference. A similar observation can be made in the case of 2-D solution as shown in Figure 17. The ventilated cavity shapes are seen

to converge rapidly towards the $Fn = \infty$ ($g = 0$) shape.

Figure 18 shows the effect of the angle of attack on the ventilated cavity shapes ($g \neq 0$ corresponds to $Fn_c = 2$). The cavity volume is seen to increase with a corresponding increase in the angle of attack. From the experimental results of [19], no ventilation is seen for angles less than 6°. For the smaller angles of attack, the fully-wetted mode can be used instead to calculate the pressure on the hydrofoil.

A comparison of the pressure distribution along the wetted face, between SPPAN (linear, negative-image method for the free-surface) and the current nonlinear method is shown in Figures 19 and 20. The linear method is clearly deficient in capturing the excess pressure due to the nonlinear free-surface effects. The difference is more pronounced when gravity is included, as shown in Figure 20. The excess pressure corresponds to the region $y > 0$ where $y = 0$ corresponds to the undisturbed free-surface level. This difference was shown to exist even in the very early stages of entry [38]. The differences in the ventilated cavity shapes predicted by the linear and nonlinear schemes is shown in Figure 21. The key difference is that the linear scheme is not able to capture the rise of the free-surface and the jets formed along the wetted boundary of the hydrofoil. As seen from the pressure distributions, it is important to capture the rise in the free-surface to get a better prediction of the pressures along with wetted boundary. Figures 19, 20 and 21 highlight the shortcomings of the negative-image method and the importance of including the nonlinear free-surface effects in the 3-D PROPCAV model.

The BEM model is based within a framework of potential flow, which neglects the real fluid effects of viscosity and surface tension. A FLUENT based RANS multiphase model (volume-of-fluid with SST $k - \omega$ turbulence model) is used to gauge the deficiencies, if any, in neglecting these effects. A detailed description of the RANS model is presented in [39]. A comparison of the ventilated surface on the suction side along with the free-surface elevation on the pressure side of the hydrofoil, as predicted by the multiphase and BEM models, is shown in Figure 21. The multiphase model predicts possible Rayleigh-Taylor instabilities on the ventilated cavity surface due to the dynamic effects of the surrounding air. This effect is not considered in the BEM scheme and in spite of this, the overall comparison between the ventilated cavity shapes predicted by the two models is good. The other difference is the peeling away of the free-surface on the pressure side of the hydrofoil resulting in the formation of spray. The BEM scheme cannot capture this as the free-surface body intersection point is kept always on the wedge surface to prevent the formation of gaps in the domain boundary. The formation of spray, however, does not affect the pressure distribution on the wetted boundary as seen in Figure 22. The comparison between the pressures predicted by the potential flow and viscous multiphase models are in excellent agreement.

In terms of CPU time, the total simulation time upto the point of comparison for the BEM scheme is about 1 hr, while for the FLUENT simulation is 50 hrs (wall-time for a parallel run with 8 nodes. Single node - 1.6 GHz AMD Opteron Dual-core processor with 4GB RAM). The above mentioned simulation times are for Δt=1e-5 s with 500 panels in the BEM scheme and approximately 460000 cells in the multiphase model. The BEM scheme has a definite advantage in predicting the ventilated cavity shapes in a fraction of the time used by the multiphase model.

Ventilating Hydrofoil - Rotational motion

The preceding section covered the vertical entry of a ventilating hydrofoil (or in general a blade element of a surface-piercing propeller). The model in essence is based on the blade-element theory (neglects the effect of the other blade elements). The flow pattern on a cylindrical surface containing the blade element is assumed to be entirely two-dimensional and this basically neglects the flow along the radial direction of the propeller. The flow on the cylinder is flattened out into a horizontal layer of water extending laterally without bound [12–14]. This simple approach works well in the case of low-advance ratios and has been traditionally used to model the entry-phase of a blade section. Simulating the exit phase requires some special treatment. [12–14] assumed the horizontal water layer to have a thickness corresponding to the distance traveled by the leading edge of the blade-element in the water during a single revolution of the propeller. This approximation makes the problem amenable to mathematical analysis.

The authors wish to take a different approach by considering the complete rotational motion of a surface-piercing hydrofoil, starting with the entry phase and culminating in the hydrofoil exiting the air-water interface. The proposed approach is as shown in Figure 24. The blade-element is a section of the propeller at a certain radius and is allowed to rotate at the propeller RPM (expressed as ω). Figures 25-28 show the preliminary results obtained using this approach. The hydrofoil (wedge-shaped) has a chord of 0.04 m and rotates at a radius of 0.1 m with ω=100 rad/s. These characteristics approximately correspond to a section of the `841-B` propeller ([4]) at a radius of 0.7 r/R. It can be seen from the figures that the scheme is able to predict the ventilated cavity shape over the entire submerged cycle of rotation. In terms of physical aspects, at this rpm, the ventilated cavity does not collapse and the suction side remains ventilated at all times. This is an ideal case scenario for the operation of a surface-piercing propeller. Some oscillations are seen at the mouth of the ventilated cavity, which require further analysis.

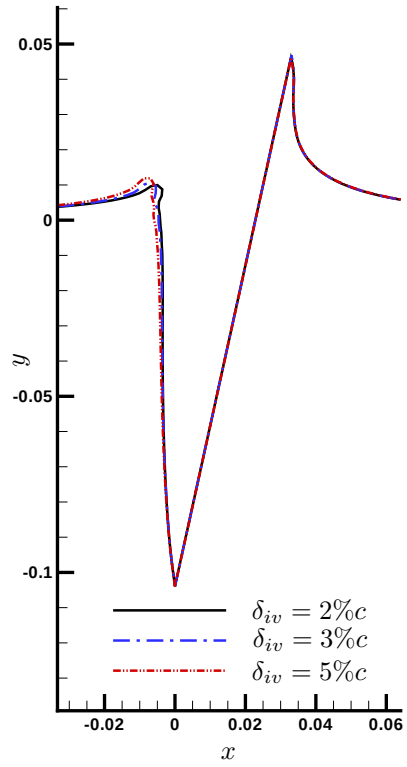

Figure 10: Effect of the length of the initial guess (δ_{iv}) of the ventilating solution on the final shape of the ventilated cavity. ($\alpha = 10°$,$g = 0$)

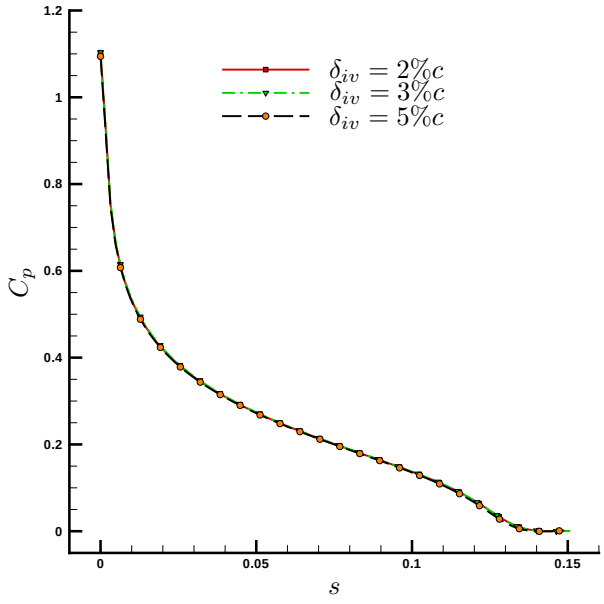

Figure 11: Effect of the length of the initial guess (δ_{iv}) of the ventilating solution on the pressure (pressure on the wetted-side of the hydrofoil). ($\alpha = 10°$,$g = 0$)

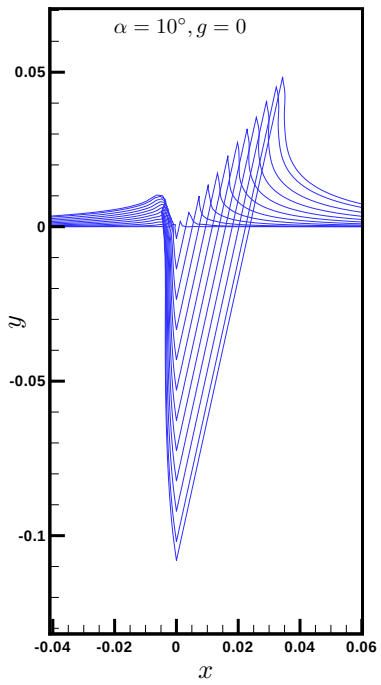

Figure 12: Ventilated cavity shapes and free-surface elevation for increasing levels of submergence. ($\alpha = 10°$,$g = 0$)

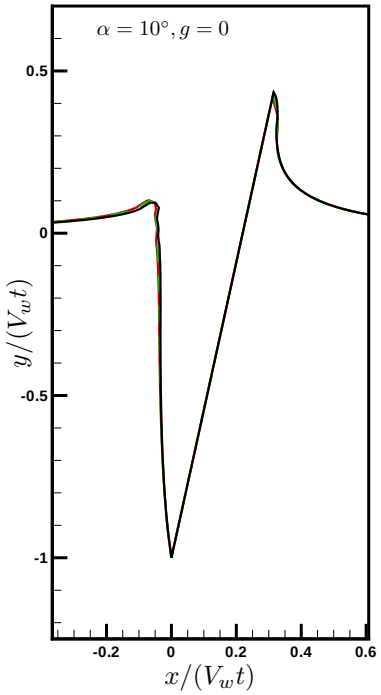

Figure 13: Ventilated cavity shapes and free-surface elevation for increasing levels of submergence expressed in terms of the similarity variables. ($\alpha = 10°$,$g = 0$)

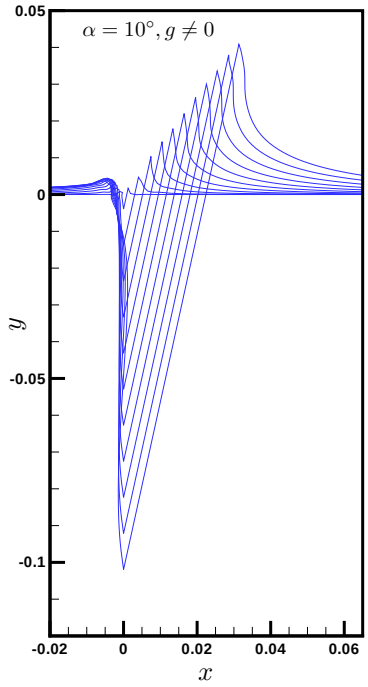

Figure 14: Ventilated cavity shapes and free-surface elevation for increasing levels of submergence. ($\alpha = 10°$,$g \neq 0$,$Fn_c = 2$)

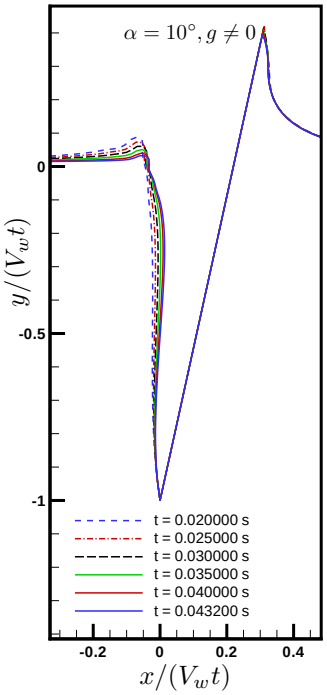

Figure 15: Ventilated cavity shapes and free-surface elevation for increasing levels of submergence expressed in terms of the similarity variables. ($\alpha = 10°$,$g = 0$,$Fn_c = 2$)

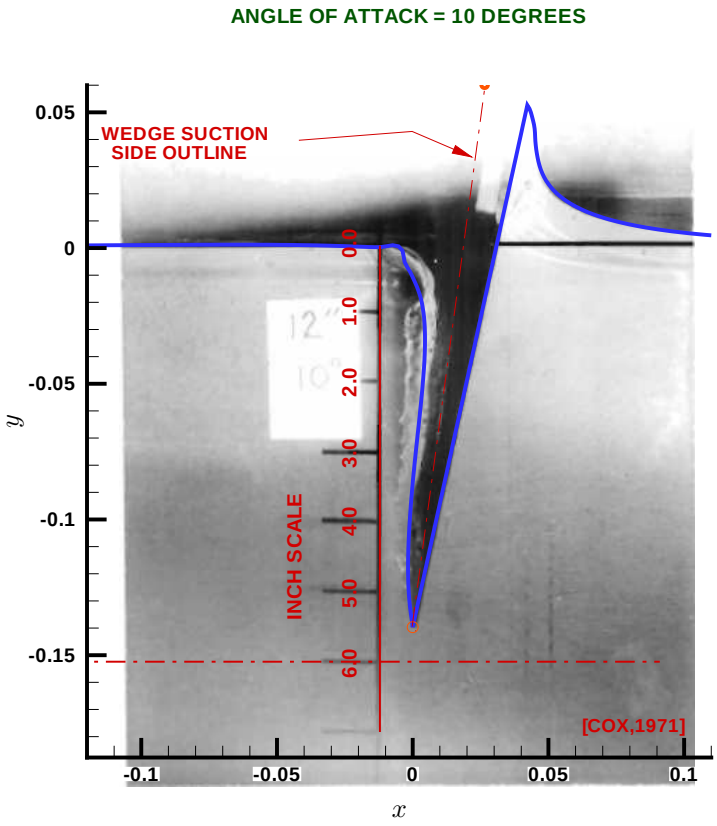

Figure 16: Comparison of numerical and experimental ventilated cavity shapes (photograph from [19])

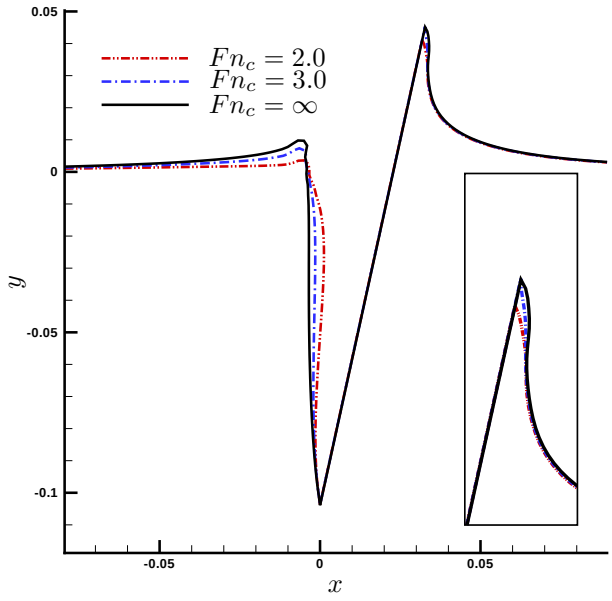

Figure 17: Effect of the Froude number on the ventilated cavity shape (inset shows the enlarged region on the wetted side of the hydrofoil)

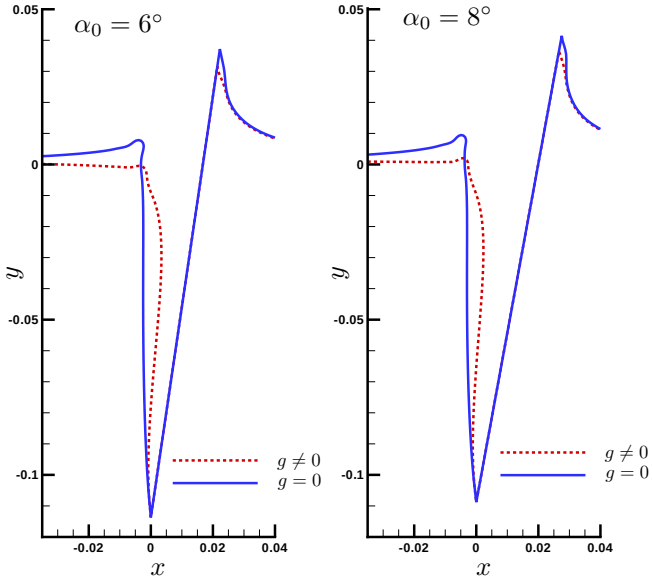

Figure 18: Effect of angle of attack on the ventilated cavity shapes (with and without the effects of gravity)

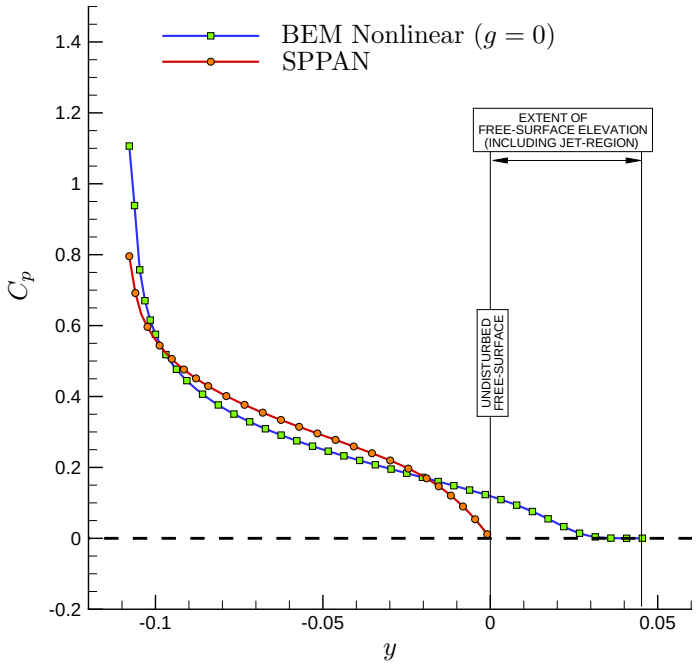

Figure 19: Comparison of pressure distribution, along the wetted face of the wedge, between SPPAN (linear) and the current method. Angle of attack $\alpha = 10°$, excluding the effects of gravity

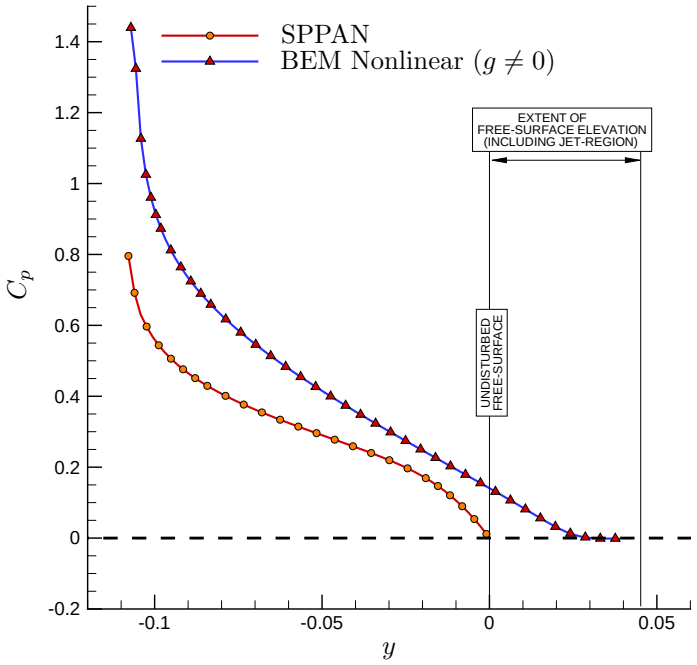

Figure 20: Comparison of pressure distribution, along the wetted face of the wedge, between SPPAN (linear) and the current method. Angle of attack $\alpha = 10°$, including the effects of gravity

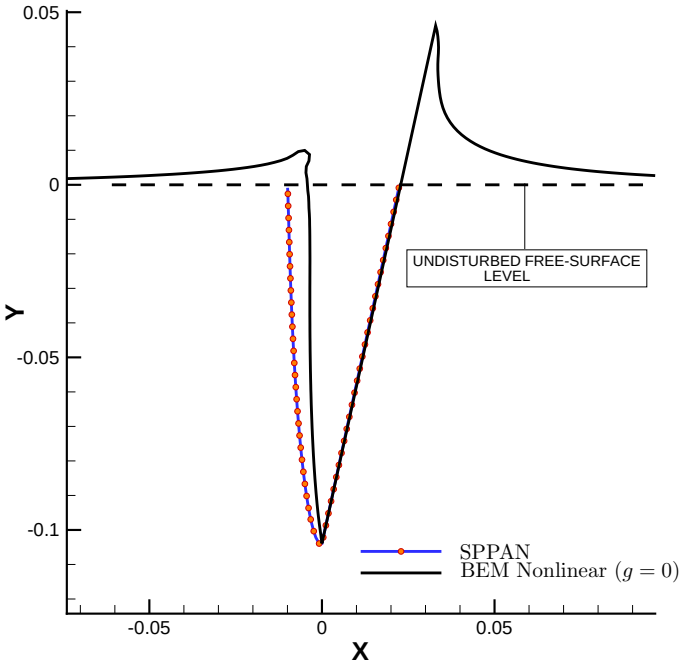

Figure 21: Comparison of ventilated cavity shapes predicted by the SPPAN (linear) and the current nonlinear method. Angle of attack $\alpha = 10°$, excluding the effects of gravity

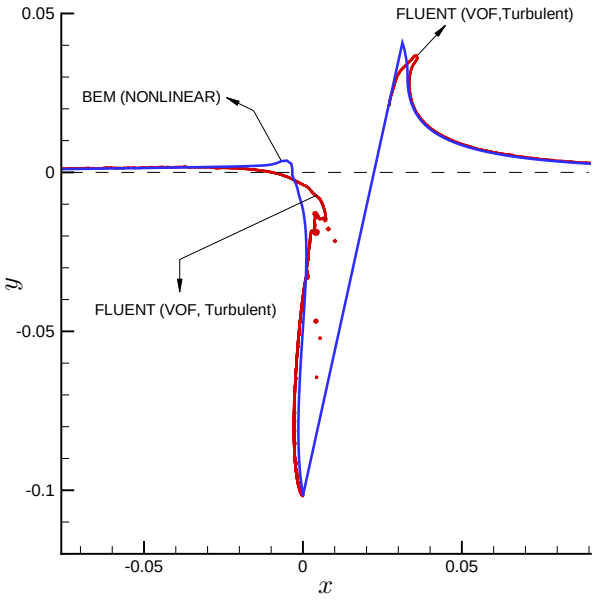

Figure 22: Ventilating entry of a surface-piercing wedge : Comparison of ventilated cavity shapes between RANSE Multiphase and BEM models. V_w=2.45 m/s. Angle of attack, α_0=10°.

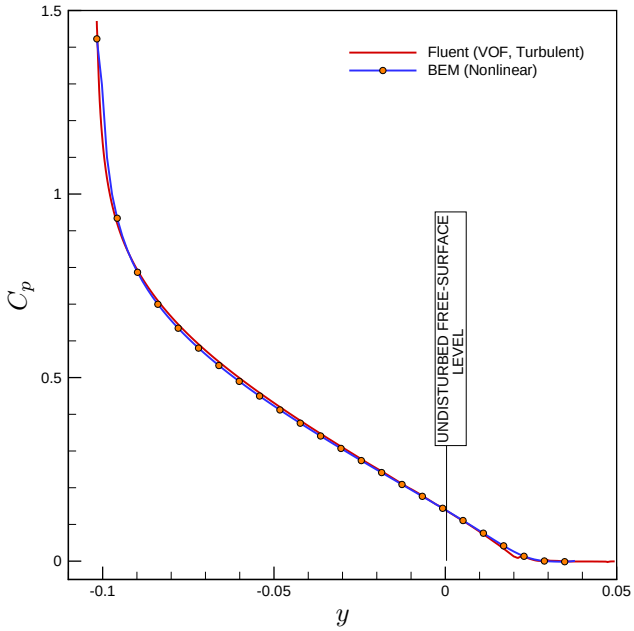

Figure 23: Ventilating entry of a surface-piercing wedge : Comparison of pressure along the wetted body surface between RANSE multiphase and BEM models. V_w=2.45 m/s. Angle of attack, α_0=10°.

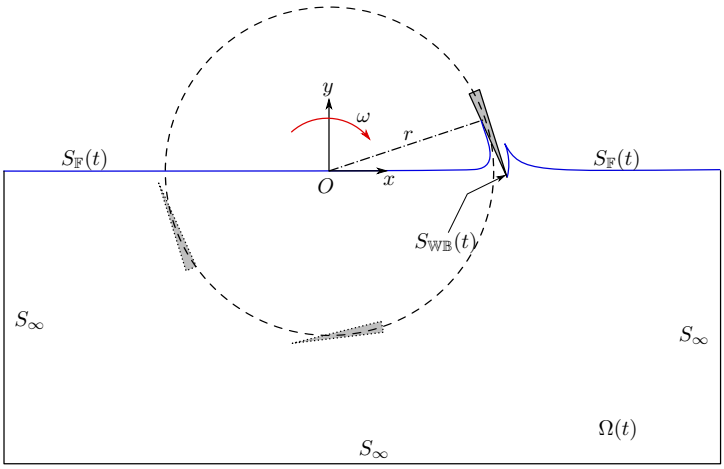

Figure 24: Rotating entry of a blade section : Fluid domain and corresponding boundaries

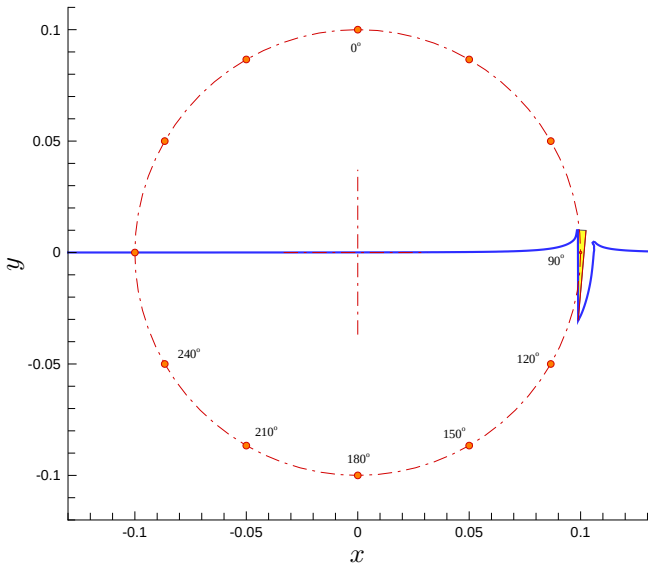

Figure 25: Surface-piercing hydrofoil in rotational motion : blade angle = 90°

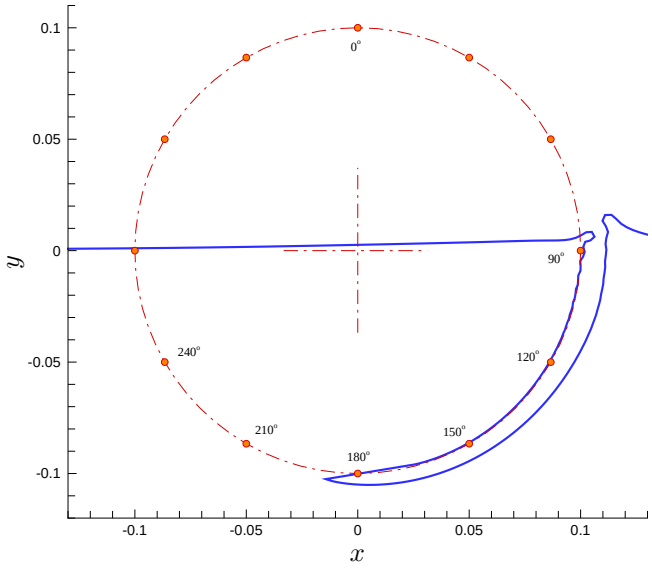

Figure 26: Surface-piercing hydrofoil in rotational motion : blade angle = 180°

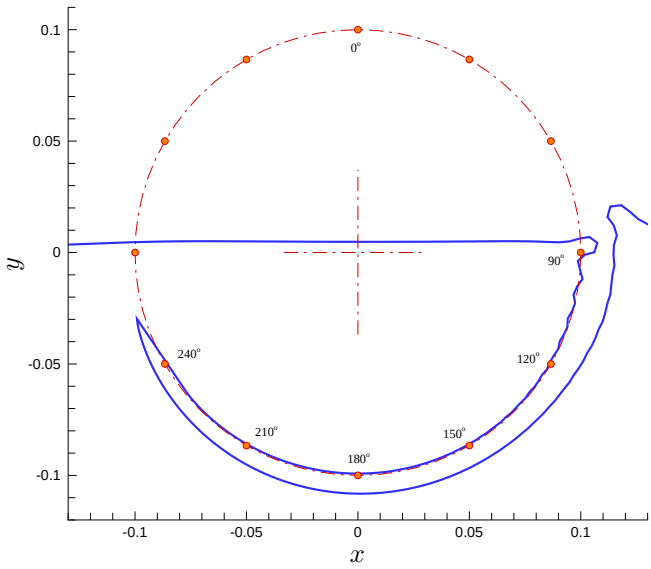

Figure 27: Surface-piercing hydrofoil in rotational motion : blade angle = 240°

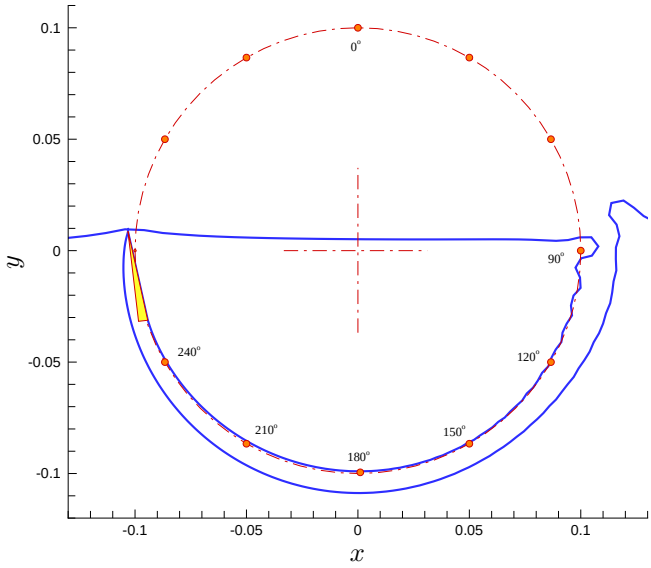

Figure 28: Surface-piercing hydrofoil in rotational motion : blade angle ≈ 260°

CONCLUSIONS

A 2D boundary element method was developed to numerically model the fully ventilated flow past a surface-piercing hydrofoil. The highlights of the scheme are the fully nonlinear free-surface boundary conditions and the ability to model the ventilated flow for arbitrary Froude numbers. The treatment of the jets formed along the wetted surface is also done in a robust manner to capture the full extent of the free-surface nonlinearities. The scheme was well validated by comparing the predicted free-surface elevations/pressures with self-similar solutions and experimental results. The BEM scheme was also extended to model the ventilating flow resulting from the rotational motion of a surface-piercing hydrofoil, which is a significant improvement over the vertical-entry scheme that models only the entry-phase. The current scheme is able to sustain the growth of the ventilated cavity over the entire cycle of submergence. The authors also plan on extending the rotating hydrofoil case to address the exit-phase. The effects of viscosity and spray on the wetted pressures were shown to be insignificant through the comparison with a RANS multiphase model.

In a nutshell, the BEM scheme presented here provides a fast and reliable way to predict the ventilated cavity shapes and helps assess the errors resulting from the linear free-surface assumptions in the modeling of surface-piercing propellers.

Extension to three dimensions

PROPCAV and its treatment of the free-surface with a negative-image method are based on a lower-order BEM. As a first step towards extending the current linear-strength scheme to PROPCAV, a constant-strength panel method was developed to model the water-entry of surface-piercing hydrofoils. The overall agreement between the linear-strength and constant-strength schemes was found to be satisfactory. Based on this conclusion, the authors are working on improving the 3D hydrodynamic model in PROPCAV by including the nonlinear free-surface boundary conditions within the existing framework of a lower-order BEM.

ACKNOWLEDGMENT

Support for this research was provided by the Office of Naval Research (Contract N00014-07-1-0932, Monitor: Ms. Kelly Cooper). The authors wish to thank Dr. Bruce Cox for sharing with them information on his experimental observations. The authors also wish to thank Dr. Alessandro Iafrati of INSEAN for his valuable comments regarding the numerical aspects of the water-entry problem.

REFERENCES

[1] Baird, N., 1998. *The World Fast Ferry Market*. Baird Publications, Melbourne, Australia.

[2] Faltinsen, O. M., 2005. *Hydrodynamics of High-Speed Marine Vehicles*. Cambridge University Press.

[3] Blount, D. L., and Bartee, R. J., 1997. "Design of propulsion systems for high-speed craft". *Marine technology,* ***34***(4), pp. 276–292.

[4] Olofsson, N., 1996. "Force and flow characteristics of a partially submerged propeller". PhD thesis, Department of Naval Architecture and Ocean Engineering, Division of Hydromechanics, Chalmers University of Technology, Götborg, Sweden.

[5] Shen, Y., 1975. "General scaling problems on fully cavitating and ventilated flows". In Proceedings of the 17th ATTC.

[6] Scherer, J., 1977. "Partially submerged and supercavitating propellers". In Proceedings of the 18th ATTC.

[7] Morgan, W., 1966. "The testing of hydrofoils for fully-cavitating or ventilated operations". In Proceedings of the 11th ITTC.

[8] Suhrbier, K., and Lecoffre, Y., 1986. "Investigation of the influences of test techniques, water speed and nucliei seeding on the characteristics of a high speed model propeller in a cavitation tunnel and correlation with full scale measurements". In International Symposium on Cavitation.

[9] Young, Y. L., 2002. "Numerical Modeling of Supercavitating and Surface-piercing Propellers (also UT-OE Report No. 02-1)". PhD thesis, Ocean Engineering Group, Department of Civil Engineering, Architectural and Evironmental Engineering, University of Texas at Austin, Austin, Texas, May.

[10] Young, Y. L., and Kinnas, S. A., 2003. "Numerical modeling of supercavitating propeller flows". *Journal of Ship Research,* ***47***(1), March, pp. 48–62.

[11] Kinnas, S. A., and Fine, N. E., 1992. "A nonlinear boundary element method for the analysis of unsteady propeller sheet cavitation". In Nineteenth Symposium on Naval Hydrodynamics, pp. 717–737.

[12] Yim, B., 1974. "Linear theory on water entry and exit problems of a ventilating thin wedge". *Journal of Ship Research,* ***18***(1), pp. pp. 1–11.

[13] Wang, D. P., 1977. "Water entry and exit of a fully ventilated foil". *Journal of Ship Research,* ***21***(1), pp. 44–68.

[14] Wang, D., 1979. "Oblique water entry and exit of a fully ventilated foil". *Journal of Ship Research,* ***23***, pp. pp. 43–54.

[15] Shiba, H., 1953. Air-drawing of marine propellers. Tech. Rep. No. 9, Transportation Technical Research Institute, Mejiro, Toshimaku, Tokyo, Japan, August.

[16] Von Karman, T., 1929. The impact of seaplane floats during landing. Tech. rep., NACA TN321.

[17] Wagner, H., 1932. "Über stoss- und gleitvorgänge an der oberflänche von flüssigkeiten". *Z. Angew. Math.*

Mech., ***12***(4), pp. pp. 192–215.

[18] Korobkin, A. A., and Pukhnachov, V. V., 1988. "Initial stage of water impact". *Annual Review of Fluid Mechanics,* ***20***(1), pp. 159–185.

[19] Cox, B. D., 1971. "Hydrofoil theory for Vertical Water Entry". PhD thesis, Department of Naval Architecture, Massachusetts Institute of Technology, May.

[20] Terent'ev, A. G., 1977. "Oblique entry of a thin body into incompressible liquid". *Izv. Akad. Nauk SSSR Mekh. Zhidk. Gaza,* ***5***, pp. 16–24.

[21] Chekin, B. S., 1989. "The entry of a wedge into an incompressible fluid". *J. Appl. Math. Mech,* ***53***(3), pp. 300–307.

[22] Faltinsen, O. M., and Semenov, Y. A., 2008. "Nonlinear problem of flat-plate entry into an incompressible liquid". *Journal of Fluid Mechanics,* ***611***, pp. 151–173.

[23] Vinayan, V., Kinnas, S. A., and Yu, Y.-H., 2005. "Modeling of the flow around FPSO hull sections subject to roll motion: Effect of nonlinear boundary conditions". *Proceedings 24th Int. Conference of Offshore Mech. and Arct. Eng.(OMAE2005), Halkidiki,Greece,* ***3***, pp. 805–815.

[24] Vinayan, V., and Kinnas, S. A., 2007. "A BEM for the propagation of nonlinear planar free-surface waves". *Electronic Journal of Boundary Elements,* ***5***(1), pp. pp 17–40.

[25] Longuet-Higgins, M. S., and Cokelet, E. D., 1976. "The deformation of steep surface waves on water. I. A numerical method of computation". *Proceedings of the Royal Society of London. Series A, Mathematical and Physical Sciences,* ***350***(1660), July 30, pp. 1–26.

[26] Savineau, C. M., 1996. "*A Time Marching Boundary Element Method for the Prediction of the Flow Around Surface Piercing Hydrofoils*". Master's thesis, Department of Ocean Engineering, Massachusetts Institute of Technology, February.

[27] Savineau, C. M., and Kinnas, S. A., 1995. "A numerical formulation applicable to surface piercing hydrofoils and propellers". In 24th International Towing Tank Conference.

[28] Dussan V., E. B., 1976. "On the difference between a bounding surface and a material surface". *Journal of Fluid Mechanics,* ***75***(4), pp. pp. 609–623.

[29] Wehausen, J. V., and Laitone, E. V., 1960. "Surface Waves". *Handbuch der Physik,* ***9***, pp. 446–778.

[30] Wu, T. Y. T., 1955. A free streamline theory for two-dimensional fully cavitated hydrofoils. Tech. Rep. Report No. 21-17, California Institute of Technology, Pasadena, California.

[31] Zhao, R., Faltinsen, O. M., and Aarsnes, J., 1996. "Water entry of arbitrary two-dimensional sections with and without flow separation". In Proceedings of 21st Symposium on Naval Hydrodynamics, National Academy Press, Washington D.C., pp. 408–423.

[32] Kihara, H., 2006. "A computing method for the flow-analysis around a primatics planing-hull". In Proc. 5th International Conference on High-Performance Marine Vehicles, pp. 262–272.

[33] Sun, H., and Faltinsen, O. M., 2007. "The influence of gravity on the performance of planing vessels in calm water". *Journal of Engineering Mathematics,* ***58***(1), pp. 91–107.

[34] Dobrovol'skaya, Z. N., 1969. "On some problems of similarity flow of fluid with a free surface". *Journal of Fluid Mechanics,* ***36***, pp. pp. 805–829.

[35] Kim, M. H., and Hong, S. Y., 2000. "Nonlinear wave forces on a stationary vertical cylinder by HOBEM-NWT". In Proc. 7th International Offshore and Polar Eng. Conf., ISOPE, Vol. 3, pp. 209–214.

[36] Dobrovol'skaya, Z. N., 1969. "On some problems of similarity flow of fluid with a free surface". *Journal of Fluid Mechanics,* ***36***(04), pp. 805–829.

[37] Zhao, R., and Faltinsen, O., 1993. "Water entry of two-dimensional bodies". *Journal of Fluid Mechanics,* ***246***, pp. 593–612.

[38] Vinayan, V., and Kinnas, S. A., 2008. "Numerical modeling of surface piercing hydrofoils and propellers". In Proceedings of the 27th Symposium on Naval Hydrodynamics.

[39] Vinayan, V., 2009. "A Boundary Element Method for the Strongly Nonlinear Analysis of Ventilating Water-entry and Wave-body Interaction Problems (also UT-OE Report No. 09-2)". PhD thesis, Ocean Engineering Group, Department of Civil Engineering, Architectural and Evironmental Engineering, University of Texas at Austin, Austin, Texas, August.